Int. J. Solids Structures Vol. 17, pp. 479–492, 1981
Printed in Great Britain.

0020-7683/81/050479-14$02.00/0
Pergamon Press Ltd.

CREEP RELAXATION OF STRESS AROUND A CRACK TIP

J. L. BASSANI
Department of Mechanical Engineering and Applied Mechanics, University of Pennsylvania, Philadelphia, PA 19104, U.S.A.

and

F. A. MCCLINTOCK
Department of Mechanical Engineering, Massachusetts Institute of Technology, Cambridge, MA 02139, U.S.A.

(*Received* 15 *August* 1980)

Abstract—Plane-strain numerical solutions have been obtained for the power-law creep relaxation of crack tip stresses subsequent to an initial elastic response. Explicit time integration is coupled with an initial-strain, finite element calculation. For cost effective, automatic time step control, the Irons-Treharne-Cormeau stable time step estimate is used to restabilize the calculation between steps 5–50 times larger. This finite element scheme is readily adaptable to realistic (and complicated) creep flow relations. Numerical results are presented for the plane-strain shallow Mode I tensile edge crack under constant applied load and creep exponents of 3 and 10. The calculated short-time amplitude of the singular HRR crack tip field under small-scale creeping conditions determines stresses that are within 1.5% of those predicted, using the elastic stress intensity factor K_I with the Riedel–Rice approximation. This precedes a longer time transition to a steady-state value that is given in terms of the path-independent integral C^*. Time-dependent crack opening displacements and velocities and the growth of regions where creep strains exceed the elastic strains are also presented.

1. INTRODUCTION

At elevated temperatures creep cracking of polycrystalline metals may progress by both pre-strain mechanisms and crack-tip mechanisms that are confined within the so-called fracture process zone[1, 2]. Pre-strain mechanisms include cavitation, strain-induced over-aging and grain boundary sliding and cracking ahead of the main crack. Crack-tip mechanisms include grain boundary cracking from the existing tip, corrosive film breakage and corrosive tunnelling. For a particular structural component the influence of nominal loading on creep crack growth is through the time-dependent stress and displacement fields that set boundary conditions on the fracture process zone, and any prior damage of material entering this zone. In this paper we are concerned with numerical methods for calculating these continuum fields without regard to the actual fracture process. The material behavior is idealized to include elastic and secondary creep response, but the methods should also apply to problems involving structural materials for which primary creep often contributes significantly to the total creep.

Recently, Riedel[3] and Riedel and Rice[4] have given solutions for the transient singular fields at the tip of a stationary crack under creep conditions. When the fracture process zone is embedded within the singular field, then a one-parameter, time-dependent amplitude factor scales the influence of geometry and nominal loading on crack growth. On the other hand, when the singular field dominates over a region that is small compared with the fracture process zone, then a more complete description than the asympototic, singular one is required (see Parks[5]). In either case, for various geometries and loadings, numerical soutions connecting the remote and crack tip fields are needed since complete analytic solutions are seldom found.

We begin Section 2 with a discussion of the creep relaxation problem under constant load and a review of the singular crack tip field. In Section 3, the cost-effective Zienkiewicz-Cormeau[6, 7] explicit time-integration scheme coupled with linear elastic finite element solutions is outlined. Automatic time step control and occasional leaps in time are also incorporated.

Numerical results are presented in Section 4 for the stress, strain and displacement fields around a shallow edge-crack under plane-strain and constant Mode I tensile loading conditions. Creep exponents of $n = 3$ and 10 are considered. Calculations for $n = 10$ required much shorter time steps and therefore much greater cost than those for $n = 3$. Comparisons are made with the short-time Riedel–Rice[4] approximation for the transient amplitude of the singular field. For times less than roughly one tenth the time it takes for nominal creep strains to equal

nominal elastic strains, the elastic stress intensity factor K_I is the relevant geometry and loading parameter that, along with time, sets this amplitude. For much longer times the path-independent integral C^* is the relevant parameter. Also presented are the time-dependent crack tip and mouth opening displacements and velocities and the growth of regions where creep strains exceed the elastic strains.

2. PROBLEM STATEMENT

Elasticity and power law creep

The total tensile strain rate $\dot{\epsilon}$, expressed as the sum of the elastic and creep strain rates, is given in terms of the uniaxial stress σ and several material constants: Young's modulus E, unit stress σ_0, creep rate $\dot{\epsilon}_0$ at the unit stress, and creep exponent n:

$$\dot{\epsilon} = \dot{\sigma}/E + \dot{\epsilon}_0 (\sigma/\sigma_0)^n. \tag{2.1}$$

The constants $\dot{\epsilon}_0$ and σ_0 are not combined into one constant ($B = \dot{\epsilon}/\sigma_0^n$ is often used) to emphasize dimensional consistency throughout. A generalization of eqn (2.1) for multiaxial stress states in terms of the deviatoric components of strain rate $\dot{\epsilon}'_{ij}$ and stress σ'_{ij} and the effective tensile stress†

$$\bar{\sigma} = \left(\tfrac{3}{2}\sigma'_{ij}\sigma'_{ij}\right)^{1/2} \tag{2.2}$$

is given by

$$\dot{\epsilon}'_{ij} = \frac{2(1+\nu)}{E}\dot{\sigma}'_{ij} + \tfrac{3}{2}\dot{\epsilon}_0 (\bar{\sigma}/\sigma_0)^{n-1}\sigma'_{ij}/\sigma_0, \tag{2.3}$$

where ν is Poisson's ratio. Dilatation is purely elastic:

$$\dot{\epsilon}_{ii} = \left(\frac{1-2\nu}{E}\right)\dot{\sigma}_{ii}. \tag{2.4}$$

The initial-boundary-value problem

The rate forms of the equilibrium and strain-displacement equations are respectively,

$$\dot{\sigma}_{ij,j} = 0, \tag{2.5}$$

$$\dot{\epsilon}_{ij} = \tfrac{1}{2}(\dot{u}_{i,j} + \dot{u}_{j,i}) \tag{2.6}$$

where u_i are the displacement components.

Initially, the plane-strain, edge-crack configuration shown in Fig. 1 is free of stress and strain. At time $t = 0$ a nominal tensile stress $\sigma_{22} = \sigma_N$ (Mode I) is suddenly applied on the circular boundary and thereafter held constant. The circular boundary centered at $x_1 = -a$, $x_2 = 0$ has a radius equal to $21a$ that was chosen to approximate an edge crack in a half space. Both the crack $-a \leq x_1 \leq 0$, $x_2 = 0$ and the surface $x_1 = -a$ are traction free. Symmetry of this Mode I configuration allows us to consider just the domain $x_2 \geq 0$, with the boundary conditions on $x_2 = 0$, $x_1 > 0$, given by $u_2 = \sigma_{12} = 0$.

Upon sudden loading, the instantaneous response is purely elastic, and the crack tip field is given by linear elastic fracture mechanics. With the load held constant subsequent creep deformation causes a *relaxation* of the crack tip stresses until, as $t \to \infty$, a steady-state stress distribution is reached (see Leckie and Ponter [8]). Higher creep rates at higher stresses cause a faster relaxation in the crack tip region than in the nominal field. Our finite element results for the shallow edge-crack show that the singular crack tip region is fully relaxed in approximately 1/10 the time it takes for creep strains to equal elastic strains in the nominal field.

Relaxation scaling relations

The solution to eqns (2.2)–(2.6) with the initial and boundary conditions (constant applied stress) stated above depends on the magnitude of loading σ_N/σ_0, the crack length a (that is taken to scale all specimen dimensions), as well as the material constants E, ν, n and $\dot{\epsilon}_0$. For numerical purposes we need only consider variations in n and ν. The solution for arbitrary values of

†Summation over repeated indices is implied.

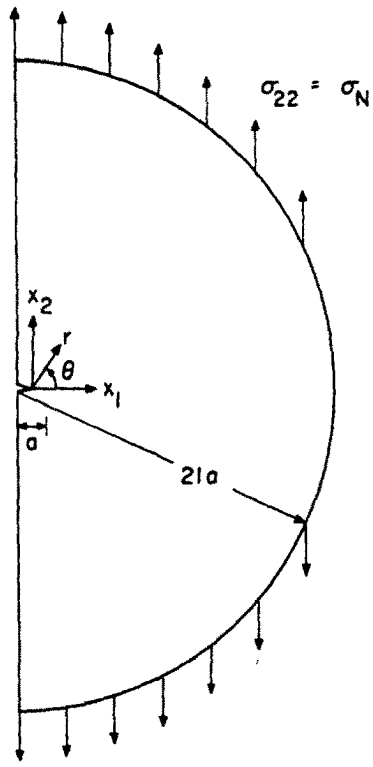

Fig. 1. Shallow edge-crack under plane-strain and constant nominal tensile stress $\sigma_{22} = \sigma_N$ loading (Mode I) conditions.

σ_N/σ_0, a, E and $\dot{\epsilon}_0$ can be found from any one solution using appropriate scaling relations. A natural time scale is

$$t_N = \frac{\sigma_N/E}{\dot{\epsilon}_0(\sigma_N/\sigma_0)^n} \equiv \frac{\epsilon_N^e}{\dot{\epsilon}_N^c}, \tag{2.7}$$

which is the time required for the creep strain to equal the elastic strain under a uniaxial tensile stress σ_N. In plane-strain tension times somewhat greater than t_N are required for the equivalent creep and elastic strains to be equal in the nominal field. This will be discussed in connection with the numerical results of Section 4.

Consider two solutions to eqns (2.2)–(2.6) that are associated with the same values of n and ν. Let superscripts 1 and 2 distinguish values of σ_N, a, E, $\dot{\epsilon}_N^c \equiv \dot{\epsilon}_0(\sigma_N/\sigma_0)^n$ and t_N associated with each solution. Then one can verify by substitution into eqns (2.2)–(2.6) that the second solution can be obtained from the first by the following scaling:

$$\sigma_{ij}^{(2)}(x_k, t) = \frac{\sigma_N^{(2)}}{\sigma_N^{(1)}} \times \sigma_{ij}^{(1)}\left(\frac{a^{(1)}}{a^{(2)}} x_k, \frac{t_N^{(1)}}{t_N^{(2)}} t\right), \tag{2.8}$$

$$\dot{\epsilon}_{ij}^{(2)}(x_k, t) = \frac{\dot{\epsilon}_N^{c(2)}}{\dot{\epsilon}_N^{c(1)}} \times \dot{\epsilon}_{ij}^{(1)}\left(\frac{a^{(1)}}{a^{(2)}} x_k, \frac{t_N^{(1)}}{t_N^{(2)}} t\right), \tag{2.9}$$

$$\dot{u}_i^{(2)}(x_k, t) = \frac{a^{(2)}}{a^{(1)}} \frac{\dot{\epsilon}_N^{c(2)}}{\dot{\epsilon}_N^{c(1)}} \times \dot{u}_i^{(1)}\left(\frac{a^{(1)}}{a^{(2)}} x_k, \frac{t_N^{(1)}}{t_N^{(2)}} t\right). \tag{2.10}$$

Substitution of eqn (2.8) into eqn (2.3) reveals that the elastic strain-rates and the creep strain-rates individually scale with the total strain-rates as given in eqn (2.9). Time integration of eqn (2.9) for constant applied stress and the appropriate scaling for the initial elastic strains gives

$$\epsilon_{ij}^{(2)}(x_k, t) = \frac{t_N^{(2)}}{t_N^{(1)}} \frac{\dot{\epsilon}_N^{c(2)}}{\dot{\epsilon}_N^{c(1)}} \times \epsilon_{ij}^{(1)}\left(\frac{a^{(1)}}{a^{(2)}} x_k, \frac{t_N^{(1)}}{t_N^{(2)}} t\right) = \frac{\sigma_N^{(2)}/E^{(2)}}{\sigma_N^{(1)}/E^{(1)}} \times \epsilon_{ij}^{(1)}\left(\frac{a^{(1)}}{a^{(2)}} x_k, \frac{t_N^{(1)}}{t_N^{(2)}} t\right). \tag{2.11}$$

Both the elastic and creep strains scale according to eqn (2.11).

Review of crack tip analysis for power law creep

At the tip of a stationary Mode I creep crack in plane strain ($\epsilon_{33} = 0$), the asymptotic stress field is of the HRR (Hutchinson–Rice–Rosengren) type[4]. In terms of the crack-tip polar coordinates r and θ, a known nondimensional function $\tilde{\sigma}_{ij}(\theta; n)$ that is normalized with the maximum over θ of $(3/2)\tilde{\sigma}_{ij}\tilde{\sigma}_{ij} = 1$, a known nondimensional function I_n in the range 3.8–6.0, and a time-dependent amplitude $C(t)$, for $t > 0$ as $r/a \to 0$

$$\sigma_{ij}^{\mathrm{HRR}}(r, \theta, t)/\sigma_0 = \left[\frac{C(t)}{\sigma_0 \dot{\epsilon}_0 a I_n}\frac{a}{r}\right]^{1/(n+1)} \tilde{\sigma}_{ij}(\theta; n). \tag{2.12}$$

On any closed path Γ surrounding the crack tip that lies within a region where the creep strain rates given by eqn (2.3) greatly exceed the elastic ones (which exists asymptotically for $t > 0$ as $r/a \to 0$)

$$C(t) = \int_\Gamma \left[\left(\frac{n}{n+1}\sigma_{ij}\dot{\epsilon}_{ij} - \sigma_{11}\frac{\partial \dot{u}_1}{\partial x_1} - \sigma_{21}\frac{\partial \dot{u}_2}{\partial x_1}\right) dx_2 + \left(\sigma_{12}\frac{\partial \dot{u}_1}{\partial x_1} + \sigma_{22}\frac{\partial \dot{u}_2}{\partial x_1}\right) dx_1\right]. \tag{2.13}$$

Integration on Γ is in a counterclockwise direction around the crack tip. As $t \to \infty$ when steady-state conditions require that $\sigma_{ij} = 0$ everywhere, $C(t) \to C^*$ and the integral in eqn (2.13) is path independent everywhere[4, 9]. Equation (2.13) is evaluated numerically from the finite element results to obtain values of $C(t)$ reported in Section 4.

For short times after an initial elastic response creep strains will dominate elastic strains only within a small crack-tip region (analogous to small-scale yielding in elastic–plastic fracture). Under these conditions, Riedel and Rice[4] found that $C(t)$ is given in terms of the elastic stress intensity factor K_I[4] That is, under constant applied stress and for times much shorter than a transition time t_T given by

$$t_T = \frac{(1-\nu^2)K_I^2}{(n+1)EC^*}, \tag{2.14}$$

then

$$\frac{C(t)}{\sigma_0 \dot{\epsilon}_0 a} \simeq \frac{(1-\nu^2)K_I^2}{(n+1)E\sigma_0 a}(\dot{\epsilon}_0 t)^{-1}. \tag{2.15}$$

Riedel and Rice[4] derived eqns (2.14) and (2.15) based on an approximate matching of the singular elastic and creep fields that assumes path independence of the J integral under small-scale creep conditions. With the standard normalizations $K_I = \hat{K}_I \sigma_N \sqrt{\pi a}$ and $c^* = \hat{C}^* \sigma_N \dot{\epsilon}_N^c a$, eqns (2.14) and (2.15) with eqn (2.7) become

$$t_T = \frac{\pi(1-\nu^2)\hat{K}_I^2}{(n+1)\hat{C}^*} t_N, \tag{2.16}$$

$$\frac{C(t)}{\sigma_N \dot{\epsilon}_N^c a} \simeq \frac{\pi(1-\nu^2)\hat{K}_I^2}{(n+1)}(t/t_N)^{-1}. \tag{2.17}$$

3. FINITE ELEMENT METHOD

An incremental finite element scheme has been developed that utilizes an automatic time stepping algorithm. Time integration is done explicitly using an Euler method that requires only an initial-strain, elastic finite element calculation[6]. The initial strains at each spatial integration point are the increment of creep strains $\Delta\epsilon_{ij}^c$ accumulated in each time step Δt and estimated from the creep strain-rate at the beginning of the step, $\Delta\epsilon_{ij}^c = \Delta t \times \dot{\epsilon}_{ij}^c(t)$. Complicated flow relations are easily adapted to explicit finite element codes.

The finite element stiffness matrix $[K]$ is then elastic and needs to be assembled and factored only once. With $\{\Delta u\}$ denoting the vector of nodal displacement-increments, $\{\Delta F^a\}$ the vector of applied nodal force-increments and $\{\Delta F^c\}$ the vector of equivalent creep force-increments, the linear finite element equations to be solved for each time step are[6]

$$[K]\{\Delta u\} = \{\Delta F^a\} + \{\Delta F^c\}. \tag{3.1}$$

The contribution of each element to ΔF^c is proportional to $AE\Delta\epsilon^c$, where A is the element area. Equation (3.1) was assembled and solved using the ADINA finite element code[10].

Finite element mesh

The final mesh used to generate the results presented in Section 4 is comprised of 216 8–node isoparametric elements. Each 8-node element has straight sides with the side nodes at the mid-points between the corner nodes. Eleven rings of elements are radially focussed at the crack tip, each with a circumferential extent $\Delta\theta = \pi/12$. The radial coordinates of each ring from the crack tip are $r/a = 0.01$, 0.013, 0.018, 0.026, 0.038, 0.057, 0.087, 0.135, 0.210, 0.331, 0.529. The inner, radially focussed part of the mesh is connected to the outer portion of the mesh shown in Fig. 2. This 716 node mesh results in 1380 degrees of freedom for which eqns (3.1) are solved.

The crack tip elements are formed by collapsing 3 nodes into 1 along one side of the 8-node element with the other side nodes remaining at the mid-points. Each of those 3 nodes can displace independently so that the interpolation function exhibits a r^{-1} singularity in displacement derivatives. This can be shown following the approach of Barsoum[11]. This is not too bad an approximation to the actual strain singularity of $r^{-n/(n+1)}$ associated with the HRR fields. On the other hand, this may not effectively model the elastic $r^{-1/2}$ singularity that exists initially ($t = 0$).

When increments of creep strain dominate increments of elastic strain, the displacement increments will be nearly incompressible. To avoid problems associated with incompressible deformations, we have used reduced (2×2) Gaussian integration within each 8-node element (Malkus and Hughes[12]).

Time-stepping algorithm, including leaping

Euler integration methods for differential equations are conditionally stable, while too large a time step can lead to unacceptable errors and even numerical overflows in the computer solution (see Ref.[13] for example). This situation is especially troublesome for so-called stiff differential equations, such as those that arise in power-law creep (especially for large n). Time steps must be much shorter than one would expect from the solution, including, for example, the stress relaxation even at points near the crack tip.

The explicit time integration (eqn 3.1) will be stable if the increment of creep strain at any integration point is at most roughly $2/n$ times the elastic strain at that point[7, 14]. An estimate of an allowable stable time-step Δt_s for power-law creep has been given by Cormeau[7]. In terms of the maximum effective stress $\bar{\sigma}_{max}$, sampled over all integration points

$$\Delta t_s = \frac{4(1+\nu)}{3n} \frac{(\bar{\sigma}_{max}/E)}{\dot{\epsilon}_0(\bar{\sigma}_{max}/\sigma_0)^n} \tag{3.2}$$

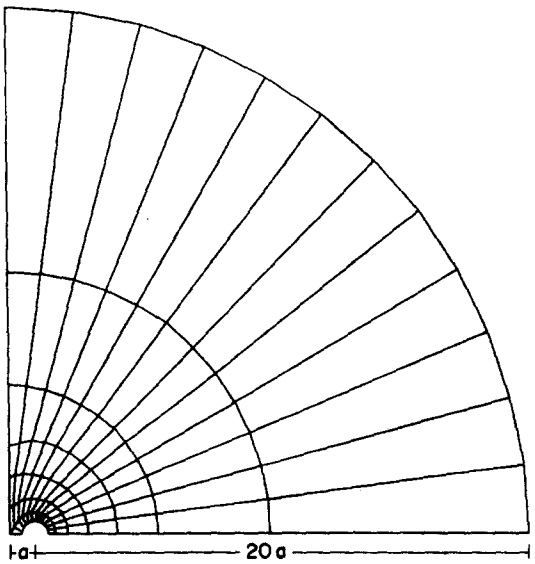

Fig. 2. Portion of the finite element mesh outside the eleven rings of radially focused elements around the crack tip.

or, with eqn (2.7)

$$\Delta t_s/t_N = \frac{4(1+\nu)}{3n(\bar{\sigma}_{max}/\sigma_N)^{n-1}}. \tag{3.3}$$

Except for a factor of $2(1+\nu)/3 \sim 1$, the result in eqn (3.2) can be derived from a one-dimensional, prototype, ordinary differential equation. This derivation is given in the Appendix.

At the end of each time step only the crack tip elements are sampled to determine $\bar{\sigma}_{max}$ and the estimate Δt_s for the next time step is calculated from eqn (3.3). For our constant load problem, the crack tip stresses are continually relaxing (decreasing) from the initial elastic values so that Δt_s tends to continually increase. In practice, time steps many times Δt_s can be taken if previous discretization errors are small. An intermittent leaping technique also proves effective where one or two steps 5–50 times Δt_s are taken followed by several shorter steps to restabilize. Our experience in generating the results summarized in Section 4 revealed that larger leaps relative to Δt_s could be taken for larger values of creep exponent n. For $n = 3, \Delta t = (5-10)\Delta t_s$ while for $n = 10$, $\Delta t = (10-50)\Delta t_s$ was used for leaping after the very short-time transient response.

A test problem

The effectiveness of incorporating the r^{-1} crack tip elements, the reduced integration, and the time-stepping algorithm was assessed by studying an HRR crack tip problem [15]. Within a semi-circular domain, a radially-focussed (6×6) mesh was used to model the crack tip. On the semi-circular boundary HRR boundary tractions, corresponding to the stresses in eqn (2.12), are applied at $t = 0$ and held constant. This problem provides a useful check of our numerical procedure since the exact steady-state solution for the stresses is known to be eqn (2.12). With the estimate Δt_s controlling the time-step size and occasional leaping, the transient response was smoothly calculated, and for long times steady state conditions ($\dot{\sigma} \simeq 0$) were observed. Both the angular and radial variations of the steady-state stresses were in good agreement, even given the coarseness of the mesh, with the HRR distribution of eqn (2.12). When excessively large leaps in time were attempted, for example with $n = 5$, $\Delta t/\Delta t_s = 20$–50, oscillations in the solution and even numerical overflows resulted. The details of this calculation will be reported in a separate paper.

4. NUMERICAL RESULTS

Some finite element results will now be presented for the edge crack ($-a < x_1 < 0$) of Fig. 1 under plane strain ($\epsilon_{33} = 0$) and constant nominal stress $\sigma_{22} = \sigma_N$ applied on the circular boundary at $t = 0$. All results are for Poisson's ratio $\nu = 0.3$, $\sigma_N = \sigma_0 = E/2000$ and either $n = 3$ or 10.

Initial elastic response

At $t = 0$ the instantaneous response is elastic. The elastic stress intensity factor computed from the J integral [16] is $K_I = 1.14\,\sigma_N\sqrt{(\pi a)}$, which is 1.5% higher than the exact result for the half space, $K_I = 1.12\,\sigma_N\sqrt{(\pi a)}$. The J integral was evaluated on several circular paths connecting integration points in the radially focussed crack tip region. This 1.5% discrepancy is due, in part, to the finite extent of the mesh and to the r^{-1} interpolation of crack tip strains instead of $r^{-1/2}$.

The highest effective stress, $\bar{\sigma}_{max}$, is always at one of the integration points nearest the crack tip. For our mesh, these integration points all lie on the semi-circular arc $r/a = 0.002$. At $t = 0$, $\bar{\sigma}_{max}/\sigma_N = 13.9$ at the integration point $r/a = 0.002$, $\theta = 63°$. From the closed-form angular variation of the elastic, singular crack tip stresses (with $\nu = 0.3$), $\bar{\sigma}$ is maximum at $\theta = 87°$, while $\bar{\sigma}$ at $\theta = 63°$ is within 7% of that value.

Initially, with all material and loading parameters except n the same, the stable-time-step estimate Δt_s *decreases* significantly with increasing n (eqn 3.3). For instance, from eqn (3.3) with $\bar{\sigma}_{max}/\sigma_N = 13.9$, at $t = 0$, $\Delta t_s(n = 10)/\Delta t_s(n = 3) \approx 10^{-5}$. Stability initially requires small time steps (which makes constant time step algorithms impractical) that steadily increase as $\bar{\sigma}_{max}$ (t) decreases.

Time steps

The initial transient response for $n = 3$ was calculated with time steps of $\Delta t/\Delta t_s = 1$ and 2. After about 10 steps when $t/t_N > 0.2$ repetitions of $\Delta t/\Delta t_s = 5,5,1,1,5,5,1,1$, etc. produced stable calculations and rapid (computer time) advance to steady-state conditions.

For $n = 10$, initial steps of $\Delta t/\Delta t_s = 1$–3 were taken. After the first ten steps and within $10^{-8} \leq t/t_N \leq 10^{-4}$, repetitions of $\Delta t/\Delta t_s = 5,5,1,1,5,5,1,1$, etc. produced stable calculations. Thereafter ($t/t_N > 10^{-4}$) very large leaps were taken followed by both short steps to restabilize the highest stressed regions and somewhat longer steps to restabilize the lower stressed regions. This scheme involved repetitions of $\Delta t/\Delta t_s = 50,1,1,5,5,1,1,5,5,1,1,50,1,1,5,5,1,1,5,5,1,1$, etc.

From calculations involving creep exponents of $n = 3, 5$ and 10 we found that as n increases, so do the allowable leaps $\Delta t/\Delta t_s > 1$ that produce stable calculations. Affordable tests for maximum allowable leaps were easily made using a restart option that was incorporated into our finite element code. All the information (e.g. nodel displacements, and integration point stresses and creep strains) required to carry on time integration was stored before each large leap. When subsequent steps showed unacceptable oscillations or an instability, the solution would be continued from the step before the leap.

Creep crack tip fields

Figure 3, for $n = 3$, shows the monotonic relaxation in 25 time steps of the amplutude of the crack tip field $C(t)$ in eqn (2.12), numerically computed from its integral representation given in eqn (2.13). Also shown is a comparison with Riedel and Rice's short time approximation given by eqn (2.17). Valeues of $C(t)$ in Fig. 3 were obtained by evaluating eqn (2.13) and finding it path independent to within one percent on at aleast 2 or 3 paths closest to the crack tip. Very short-time ($t/t_N = 10^{-5} - 10^{-4}$) values of $C(t)$ for $n = 3$ could not be found from eqn (2.13) since the region, where creep strain-rates dominated the elastic ones was to small relative to the finite element mesh. For somewhat longer times, $C(t)$ was still path dependent on all paths chosen, but values were determined based on an extrapolation of $C(t;$ path radius) to a path radius equal to zero. This technique reproduced the initial $1/t$ decay in $C(t)$ of eqn (2.17), that smoothly connected path-independent values at larger t. As time increases, so does the region around the crack tip within which $C(t;$ path radius) is nearly path independent. For $n = 3$, at $t/t_N = 0.025$, $C(t)$ computed from the Riedel–Rice approximation, eqn (2.17) with $\hat{K}_I = 1.14$ is 6% higher than the numerically computed (path independent) value from eqn (2.13). At $t/t_N = 2.5$, $C/\sigma_N \dot{\epsilon}_N^c a = 4.10$. With eqn (2.16) this provides the estimate of $t_T/t_N = 0.23$.

The relaxation of $\bar{\sigma}_{max}/\sigma_N$ for $n = 3$ is also plotted in Fig. 3. For all $t/t_N > 0.005$ this maximum occurred along $\theta = 78°$ at $r/a = 0.002$. From the angular variation of the HRR stress field, for $n = 3$ $\bar{\sigma}$ is maximum at $\theta = 95°$, while $\bar{\sigma}$ at $\theta = 78°$ is within 3% of its maximum. These numerically computed values of $\bar{\sigma}_{max}/\sigma_N$ are the ones that limited Δt_s in eqn (3.2). Note, for

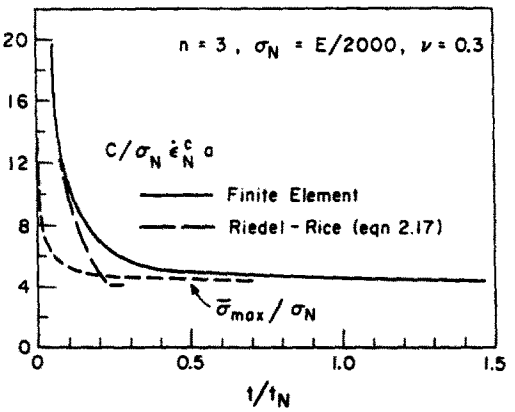

Fig. 3. Relaxation for $n = 3$ of the amplitude of the crack tip field $C(t)$ obtained from the finite element results and a comparison with eqn (2.17). Also shown is the relaxation of $\bar{\sigma}_{max}/\sigma_N$ sampled at the integration points.

example, that a factor of 2 decrease in $\bar{\sigma}_{max}$ when $t/t_N = 0.05$ corresponds to a factor of 4 increase in Δt_s. The steady-state value ($t \to \infty$) of $\bar{\sigma}_{max}/\sigma_N = 4.28$ for our mesh.

Relaxation to steady-state creep from the initial elastic field for $n = 10$ requires significantly smaller time steps than the $n = 3$ case. Recall that at $t = 0$, Δt_s ($n = 10$)/Δt_s($n = 3$) $\approx 10^{-5}$. Figure 4 includes a plot of $C(t)$ for $n = 10$ and a comparison with eqn (2-17). To reach $t/t_N = 0.66$, at which time $\bar{\sigma}_{max}/\sigma_N = 1.77$ and $\Delta t_s/t_N \approx 10^{-3}$, required 184 time steps. The $1/t$ decay of $C(t)$, which is exact for short times, provides a useful check of the numerical accuracy. For short times ($t/t_N = 10^{-5} - 10^{-4}$), eqn (2.17) determines a value of $C(t)$ that is roughly 10% higher than the numerically computed value using eqn (2.13). At $t/t_N = 0.66$, $C/\sigma_N \dot{\epsilon}_N^c\, a = 4.31$. With eqn (2.16) this provides an estimate of $t_T/t_N = 0.08$. Also shown in Fig. 4 is the relaxation of $\bar{\sigma}_{max}/\sigma_N$ that limited Δt_s in eqn (3.3). For all times plotted, this maximum occurred in the range $78° \leq \theta \leq 93°$.

Crack openings

The rate of crack-mouth opening $\dot{\Delta} = \dot{u}_2(x_1 = -a, x_2 = 0, t)$ and a measure of the rate of crack tip opening $\dot{\delta} = \dot{u}_2(x_1 = -0.01a, x_2 = 0, t)$ are shown in Figs. 5 and 6 for $n = 3$ and 10, respectively. (A measure of crack opening displacement that is often used in time-independent elastic–plastic fracture is $u_2(r, \theta = 180°)$ at $r = u_2$. Under steady-state creep conditions the rate of change of this measure is not constant, therefore it is not incorporated here.) Initially, the high crack tip stresses cause a faster rate of crack tip opening as compared with the rate of crack mouth opening. Subsequently, as the crack tip region approaches nearly complete relaxation, $\dot{\Delta}$ exceeds $\dot{\delta}$. For $n = 3$, at $t/t_N = 2.5$, $\dot{\delta}/a\dot{\epsilon}_N^c = 0.72$ and $\dot{\Delta}/a\dot{\epsilon}_N^c = 2.42$. For $n = 10$, at $t/t_N = 0.66$, $\dot{\delta}/a\dot{\epsilon}_N^c = 1.38$ and $\dot{\Delta}/a\dot{\epsilon}_N^c = 2.56$.

The crack mouth opening $\Delta = u_2(x_1 = -a, x_2 = 0, t)$ and crack tip opening $\delta = u_2(x_1 = -0.01a, x_2 = 0, t)$ are shown in Figs. 7 and 8 for $n = 3$ and 10, respectively. The initial ($t = 0$) elastic displacements $\Delta_e = 1.35 \times 10^{-3}\, a$ and $\delta_e = 1.51 \times 10^{-4}\, a$ are used for normalization. At $t/t_N = 0.66$, which is roughly the time when the magnitude of the nominal creep and elastic strains are equal, for $n = 3$, $\delta/\delta_e = 3.44$ while the observable $\Delta/\Delta_e = 1.70$. At this same normalized time for $n = 10$, $\delta/\delta_e = 7.18$ and $\Delta/\Delta_e = 1.77$. This reveals the greater crack tip deformation, relative to far field deformation, for materials with higher creep exponent n. At $t/t_N = 2.5$ for $n = 3$, $\delta/\delta_e = 7.84$ and $\Delta/\Delta_e = 2.56$.

Creep zones

The creep-zone bundary is defined as the locus of points encircling the crack tip where the equivalent creep strain $\bar{\epsilon}^c$ equals the equivalent elastic strain $\bar{\epsilon}^e$, with ($\bar{\epsilon} = (2/3\, \epsilon'_{ij}\, \epsilon'_{ij})^{1/2}$). This definition, which is arbitrary as compared with plastic zones associated with a yield criterion, has been used by Riedel[3] and Riedel and Rice[4]. Creep zones propagate outward from the

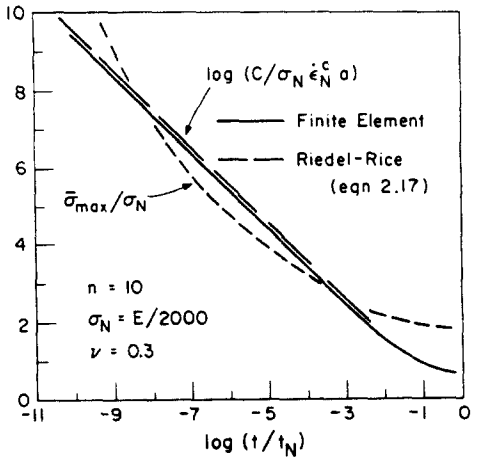

Fig. 4. Relaxation for $n = 10$ of the amplitude of the crack tip field $C(t)$ obtained from the finite element results and a comparison with eqn (2.17). Also shown is the relaxation of $\bar{\sigma}_{max}/\sigma_N$ sampled at the integration points.

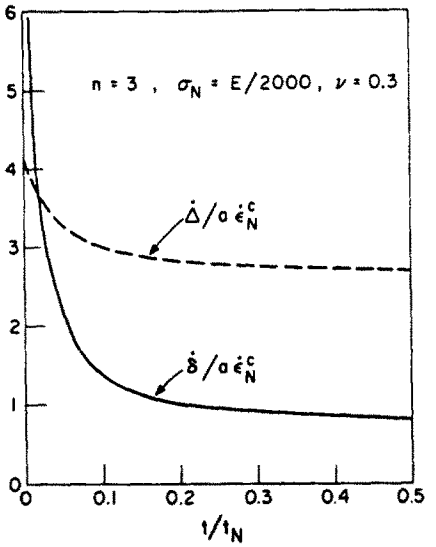

Fig. 5. Relaxation for $n = 3$ of the rate of crack mouth opening $\dot{\Delta} = \dot{u}_2(x_1 = -a, x_2 = 0, t)$ and rate of crack tip opening $\dot{\delta} = \dot{u}_2(x_1 = -0.01a, x_2 = 0, t)$.

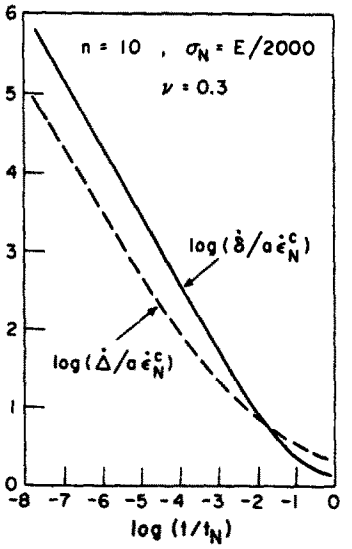

Fig. 6. Relaxation for $n = 10$ of the rate of crack mouth opening $\dot{\Delta} = \dot{u}_2(x_1 = -a, x_2 = 0, t)$ and rate of crack tip opening $\dot{\delta} = \dot{u}_2(x_1 = -0.01a, x_2 = 0, t)$.

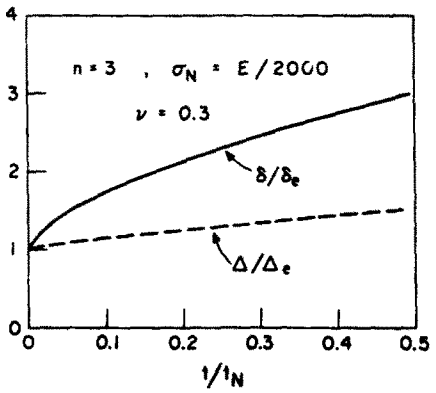

Fig. 7. For $n = 3$, total crack mouth opening Δ and crack tip opening δ, each normalized by the initial elastic values Δ_e and δ_e, respectively.

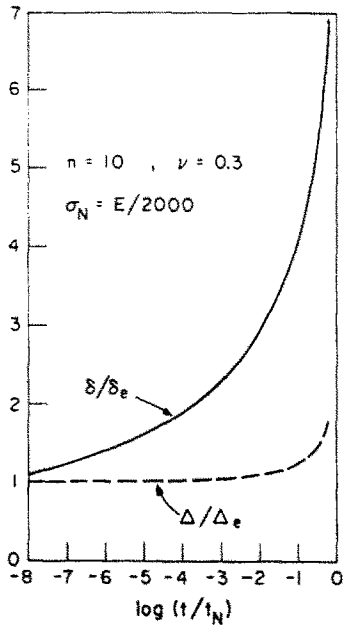

Fig. 8. For $n = 10$, total crack mouth opening Δ and crack tip opening δ, each normalized by the initial elastic values Δ_e and δ_e, respectively.

crack tip as time increases. A linear interpolation of the strains at the finite element integration points is used to construct smooth boundaries.

The time $\bar{t}_N$ when, under plane-strain tension, the creep zone extends to the nominal field, i.e. $\bar{\epsilon}_N^c(\bar{t}_N) = \bar{\epsilon}_N^e(\bar{t}_N)$, is greater than the uniaxial tension transition time t_N under the same maximum principal stress σ_N. For plane-strain tension ($\sigma_{22} = \sigma_N$, $\epsilon_{33} = 0$) one can readily show using the elastic stress-strain relations that $\bar{\sigma}_N = \sigma_N\sqrt{1 - \bar{\nu} + \bar{\nu}^2} < \sigma_N$, where $\bar{\nu}(t)$ is an effective Possion's ratio, i.e. $\sigma_{33}(t) = \bar{\nu}\sigma_N$. Similarly, $\bar{\epsilon}_N^e = (2/3)(1 + \bar{\nu})\,\bar{\sigma}_N/E$. At $t = 0$, $\bar{\nu} = \nu = 0.3$ for our results so that $\bar{\sigma}_N = 0.889\ \sigma_N$ and $\bar{\epsilon}_N^e = 0.770\ \sigma_N/E$, whereas at $t = \infty$, $\bar{\nu} = 0.5$so that $\bar{\sigma}_N = 0.866\ \sigma_N$ and $\bar{\epsilon}_N^e = 0.866\ \sigma_N/E$. Now, for $\nu = 0.3$, if we take a long time value of $\bar{\epsilon}_N^e = 0.85\ \sigma_N/E$ and a mean value of $\bar{\sigma}_N = 0.86\ \sigma_N$, then from $\bar{\epsilon}_N^e = \bar{\epsilon}_N^c = \dot{\epsilon}_0(\bar{\sigma}_N/\sigma_0)^n\ \bar{t}_N$ and eqn (2.7) we find $\bar{t}_N/t_N \simeq 0.85/0.86^n$, which equals 1.3 for $n = 3$ and 3.8 for $n = 10$. These estimates agree well with our numerical results.

Figure 9 shows short-time creep zones for $n = 3$ and $n = 10$. These zones that propagate roughly with a self-similar shape (resembling the time-independent plastic zones under small-scale yielding conditions, e.g. Shih[17] Rice and Tracey[18]), are extended further in front of the crack tip than the small-scale-creep zones approximately constructed by Riedel and Rice[4].

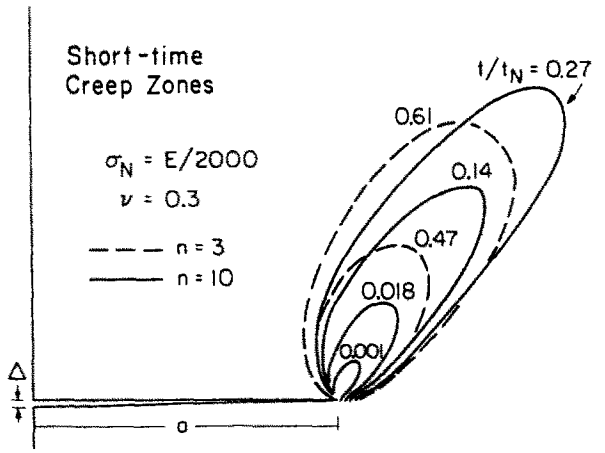

Fig. 9. Short-time creep zones where $\bar{\epsilon}^c > \bar{\epsilon}^e$ for $n = 3$ and 10.

Their self-similar zones result from the $1/t$ relaxation of $C(t)$ in eqn (2.15) and an approximate matching of the creep and elastic singular crack tip fields.

The maximum extent of the creep zones in Fig. 9 is roughly along the ray $\theta = 60°$. At a given normalized time the maximum extent of these zones increases with increasing n, while for a given extent the maximum width of these zones decreases with increasing n.

Long-time creep zones for $n = 3$ are plotted in Fig. 10. Up to $t/t_N = 1.3 \simeq \bar{t}_N/t_N$, the creep zones propagate with a more or less self-similar shape. Thereafter the zones approach the circular boundary and loose their self-similar shape. At $t/t_N = 1.6$, $\bar{\varepsilon}^c > \bar{\varepsilon}^e$ everywhere except within two narrow regions: one above and below and one directly in front of the crack. Finally, at $t/t_N = 2.5$, $\bar{\varepsilon}^c > \bar{\varepsilon}^e$ everywhere except in wedge shape regions above and below the crack.

Figures 11 and 12, for $n = 3$ and 10 respectively, are plots of the radial variation of the equivalent creep strain along two rays: one ahead of the crack, $\theta = 3°$ and the other at the maximum extent of the creep zone, $\theta = 57°$. At the times $t/t_N = 0.66$ and 2.5 for $n = 3$, straining along $\theta = 57°$ is roughly an order of magnitude more intense than straining along $\theta = 3°$ for $0.01 \leq r/a \leq 0.5$, whereas from the analytical HRR solution, as $r/a \to 0$, $\bar{\varepsilon}^c(\theta = 57°) \simeq 35 \times \bar{\varepsilon}^c(\theta = 3°)$. The nominal creep strains for $n = 3$ at $t/t_N = 0.66$ and 2.5 are $\bar{\varepsilon}_N^c = 0.00023$ and 0.00082, respectively. For $n = 10$, at $t/t_N = 0.66$ when $\bar{\varepsilon}_N^c = 0.0001$, straining alsong $\theta = 57°$ is roughly 1–2 orders of magnitude more intense than straining along $\theta = 3°$ for $0.01 \leq r/a \leq 2.0$,

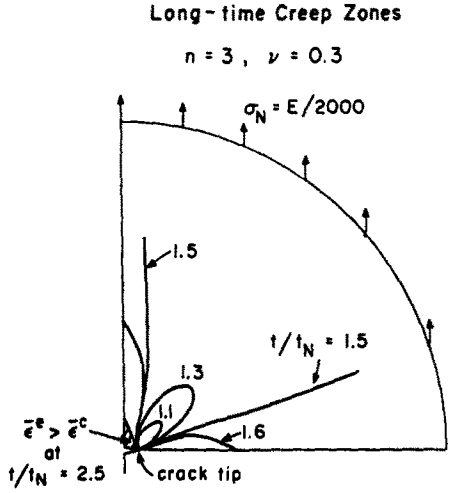

Fig. 10. Long-time creep zones where $\bar{\varepsilon}^c > \bar{\varepsilon}^e$ for $n = 3$.

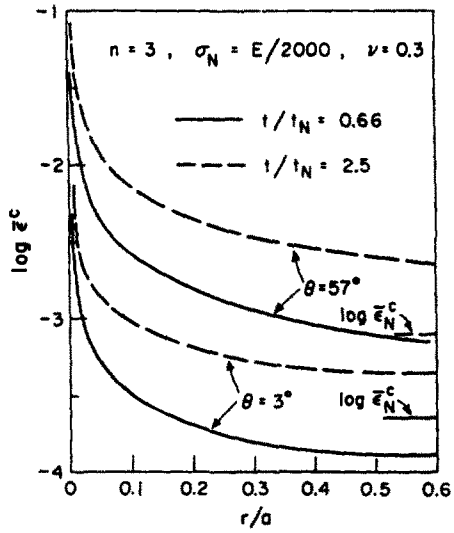

Fig. 11. Radial variation of equivalent creep strain along two rays for $n = 3$ at $t/t_N = 0.66$ and 2.5.

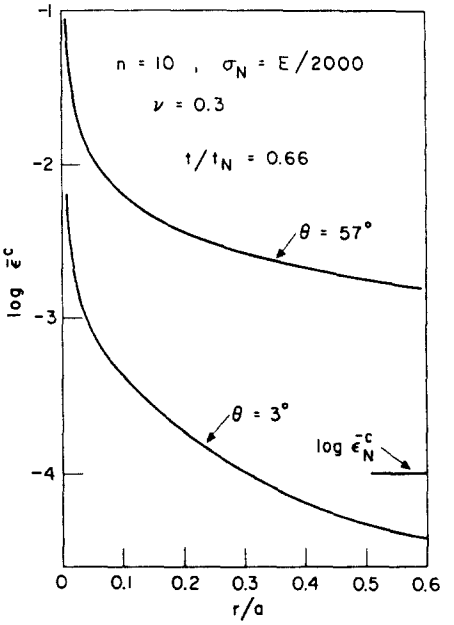

Fig. 12. Radial variation of equivalent creep strain along two rays for $n = 10$ at $t/t_N = 0.66$.

and as $r/a \to 0$, $\bar{\epsilon}^c(\theta = 57°) \simeq 20 \times \bar{\epsilon}^c(\theta = 3°)$. Both Figs. 9 and 10 show the existence of a region directly ahead of the crack, $\theta \simeq 0$ and $r/a \gtrsim 0.1$, where the accumulation of creep strain is slower than that in the nominal field.

5. DISCUSSION

Explicit time-integration coupled with automatic time-step control and occasional leaping has proven effective in calulating the transient fields around a crack tip even when stresses at the spatial integration points associated with the finite element discretization vary by more than an order of magnitude. Stability requirements, on the other hand, show a trade-off between the allowable time step and spatial refinement; that is, as the crack-tip element size is decreased for accuracy, the stresses at the integration points nearest the crack tip increase and Δt_s (eqn 3.3) decreases. For example, if the radial variation of crack tip stresses is given by eqn (2.12), then halving the size of the crack tip elements while retaining the same spatial-integration rule cause a factor of $2^{(n-1/n+1)}$ decrease in Δt_s or roughly the same factor increase in computational cost.

Our experience in calculating the short-time-transient response, $t/t_N \ll 0.1$, indicated that the stable time step is a good measure of the time step needed for accuracy. In this regime, increasing Δt far above Δt_s would lead to problems of accuracy as well as those of stability. The latter is characterized by large oscillations in stresses or even numerical overflows. This suggests that implicit time-integration methods such as the Hughes–Taylor algorithm[19] may not be cost effective for calculating the short-time response. The long-time response that approaches steady-state conditions would, on the other hand, be best calculated using an implicit algorithm so that very large time steps can be taken. Recall that for $n = 10$ at $t/t_N = 0.66$, when steady-state conditions are nearly reached, $\Delta t_s/t_N \simeq 10^{-3}$.

The calculated short-time (small-scale-creep) amplitude $C(t)$ of the crack tip field relaxed like $1/t$ (Figs. 3 and 4) as given in eqn (2.17) for times roughly less than the transition time t_T given in eqn (2.16). In this regime the rate of deformation in the far field is considerably slower than that at the crack tip (Figs. 5–8). For the shallow edge-crack and, for instance, for the center-cracked panel in tension with a crack that is short relative to panel width[20], $t_T \simeq t_N/(n+1)$. For deeper cracks in tension t_T/t_N decreases. Numerical integration of eqn (2.13) within the crack tip region using the finite element results gave values of $C(t)$ that were 5–10% lower than the Riedel–Rice approximation in eqn (2.17).

Creep straining is a maximum at roughly 60° from the crack plane (Figs. 7–10), while there is a region ahead of the crack ($0.1 \leq r/a \leq 1.0$) where creep strains fall below the nominal values. This raises the question of whether the crack should extend (locally) straight ahead or in a

zig-zag, especially when the growth and coalescence of cavities is the mechanism for crack extension[1]. The effect of increased straining above the crack tip is countered by the elevation of hydrostatic tension directly ahead, along $\theta = 0$ (see, for instance[21]). Our results for $n = 3$ and 10 predict a 15–20% evelation at $r/a = 0.1$ and a 5 – 10% evleation at $r/a = 1.0$.

Our results should help to provide guidelines for the correlation of creep crack-growth data, especially concerning the relevance of K_I or C^* (see, for instance[9]). As suggested by Riedel and Rice[4] and confirmed here, for $t < t_T$ then K_I is the relevant loading parameter, while for $t > t_T$ then it is C^*. Near the time t_T a smooth transition from K_I to C^* control occurs. The value of t_T in eqn (2.16) corresponding to particular specimen and loading conditions is determined from the material constants as well as the solutions to elastic and steady-state creep boundary value problems (see, for instance[20]). If the latter information is not available for a particular specimen configuration then estimates of the nominal creep strains as a function of time can be found from a knowledge of the nominal stresses and creep properties. Recall that for the shallow edge crack $(n + 1)$ $t_T \simeq t_N$ or $\bar{t}_N$, the times when nominal creep and elastic strains are equal. Direct measurement of the nominal creep strains, which may be difficult, and a comparison with the nominal elastic strains would also provide the necessary guidelines. This latter approach does not require material property idealization and, in particular, the neglect of primary creep strains. Riedel[22] and McClintock and Bassani[2] have discussed the relevant loading parameters when primary creep is important.

Acknowledgement—This research was supported by the U.S. Department of Energy under Contract No. EG77-S-02-4461. We are grateful to Prof. H. Riedel and Messrs. C. W. Lau and M. Snyder for helpful discussions during the early part of this study.

REFERENCES

1. A. S. Argon, I. -W. Chen and C. W. Lau, Intergranular caviation in creep: theory and experients. In *Creep and Fatigue Fracture* (Edited by R. M. N. Pelloux and N. Stoloff). AIME New York (1980).
2. F. A. McClintock and J. L. Bassani, Problems in environmentally-affected creep crack growth. In *Proc. IUTAM Symp. on Three-Dimensional Constitutive Relationships and Ductile Fracture*. Dourdan, France (1980).
3. H. Riedel, Cracks loaded in anti-plane shear under creep conditions. *Z. Metallkunde* **69**, 755–760 (1978).
4. H. Riedel and J. R. Rice, Tensile cracks in creeping solids, In *ASTM STP* 700. American Society for Testing and Materials, Philadelphia (1980).
5. D. M. Parks, The dominance of the crack tip fields of inelastic continuum mechanics. In *Proc. 2nd Int. Conf. on Num. Meth. in Fracture Mech.*, Swansea (1980).
6. O. C. Zienkiewicz and I. C. Cormeau, Visco-plasticity–plasticity and creep in elastic solids—a unified numerical solution approach. *Int. J. Num. Meth. Engng.* **8**, 821–845 (1974).
7. I. C. Cormeau, Numerical stability in quasi-static elasto-visco-plasticity. *Int. J. Num. Meth. Engng.* **9**, 109–127 (1975).
8. F. A. Leckie and A. R. S. Ponter, Deformation bounds for bodies which creep in the plastic range. *ASME J. Appl. Mech.* **37**, 426–430 (1970).
9. J. D. Landes and J. A. Begley, A fracture mechanics approach to creep crack growth, *ASTM STP* 590 pp. 128–148. American Society for Testing and Materials, Philadelphia (1976).
10. K. J. Bathe, A finite element program for automatic dynamic incremental nonlinear analysis, Report 82448–2, Acoustics and Vibration Lab, Mechanical Engineering Dept., Massachusetts Institute of Technology, Cambridge (1976).
11. R. S. Barsoum, triangular quarter-point elements as elastic and perfectly-plastic crack tip elements. *Int. J. Num. Meth. Engng.* **11**, 85–98 (1977).
12. D. S. Malkus and T. J. R. Hughes, Mixed finite element methods—reduced and selective integration techniques: a unification of concepts, *Comp. Meth. Appl. Mech. Engng* **15**, 63–81 (1978).
13. G. Dahlquist and A. Björck, *Numerical Methods*, Chapter 8. Prentice Hall, Englewood Cliffs, New Jersey (1974).
14. B. Irons and G. Treharne, A bound theorem in eigenvalues and its practical applications. *Proc. 3rd Conf. Matrix Meth. Struct. Mech.* pp. 245–254. Wright-Patterson A. F. B., Ohio (1973).
15. A. S. Argon and F. A. McClintock, Micromechanical modeling of microstructural damage in creeping alloys. MIT Progress Report for Dept. Of Energy, Materials Science Program, Contract EG-77-S-02-4461. A001 (April 1979).
16. J. R. Rice, A path independent integral and the approximate analysis of strain concentrations by notches and cracks. *ASME J. Appl. Mech.* **35**, 379–386 (1968).
17. C. F. Shih, Small scale yielding analysis of mixed mode plane-strain crack problems. *ASTM STP* 560, pp. 187–210. American Society for Testing and Materials, Philadelphia (1974).
18. J. R. Rice and D. M. Tracey, Computational fracture mechanics. *Numerical and Computer Methods in Structural Mechanics* (Edited by S. J. Fenves), pp. 585–625. Academic Press, New York (1971).
19. T. J. R. Hughes and R. L. Taylor, Unconditionally stable algorithms for quasi-static elasto/visco-plastic finite element analysis. *Comput. Structures* **8**, 169–173 (1978).
20. J. W. Hutchinson, A. Needleman and C. F. Shih, Fully plastic crack problems in bending and tension. *Fracture Mechanics* (Edited by N. J. Perrone *et al.*) pp. 515–528. University Press of Virginia, Charlottsville (1978).
21. B. Budiansky, J. W. Hutchinson and S. Slutsky, Void growth and collapse in viscous solids. *Div. Appl. Sci. Report Mech*–15, Harvard University, Cambridge, Mass (1980).
22. H. Riedel, Creep deformation at crack tips in elastic-viscoplastic solids. *Brown University Report MRL E*-114, Providence (1979).

APPENDIX

Cormeau[7] has shown that numerical spatial integration of the finite element equations (Ref.[7], eqn 1) coupled with the rate form of the stress-strain equations (Ref.[7], eqn 5) leads to a system of ordinary differential equations (Ref.[7], eqn 12) for the stresses at the integration points. Specifically, this system arises from: (1) solving eqn (3.1) for $\{\dot{u}\} = \{\Delta u\}/\Delta t$, which after numerical integration involves stresses at the spatial integration points, (2) solving for $\dot{\epsilon}_{ij}$ in eqn (2.6) at each integration point using the element interpolation functions, and finally(3) substituting into $\dot{\sigma}_{ij} = E(\dot{\epsilon}_{ij} - \dot{\epsilon}^c_{ij})$ using eqns (2.2)–(2.4) evaluated at each integration point. The total number of equations in this system equals the number of integration points times the number of independent stress components. Cormeau then bounds the eigenvalue with the largest magnitude $|\lambda_{max}|$ for this system of ODE's and requires that $\Delta t_s < 2/|\lambda_{max}|$. Except for the factor $2(1+\nu)/3$ in eqn (3.2) the essence of the approximation for Δt_s can be understood from consideration of a prototype ODE.

Cinsider the ODE

$$\frac{dy}{dt} + A\,y^n + B = 0 \tag{A1}$$

where A is a constant and B is a function of time. This ODE is a prototype for the aforementioned system of ODE's that result in elastic-power-law creep finite element analysis, where y is a stress-like quantity, $\bar{\sigma}$ say, A is proportional to $E\dot{\epsilon}_0/\sigma_0^n$ and B is proportional to the rate of applied force divided by element cross-sectional area, $\dot{F}^a/A$.

Let $y_k \equiv y(t_k)$ so that $y_{k+1} = y(t_k + \Delta t)$. The Euler tangent-method approximation (see Ref.[13]) to eqn (A1) gives the difference equation

$$\frac{y_{k+1} - y_k}{t_{k+1} - t_k} = -Ay_k^n - B \tag{A2}$$

or

$$y_{k+1} = y_k - \Delta t(Ay_k^n + B). \tag{A3}$$

Let

$$y = \bar{y} + \epsilon \tag{A4}$$

where ϵ is a local error or perturbation from the "exact" solution $\bar{y}$ that approximately satisfies eqn (A2). Then substitution of eqn (A4) into eqn (A3) gives

$$\bar{y}_{k+1} + \epsilon_{k+1} = \bar{y}_k + \epsilon_k - \Delta t\,[A\,\bar{y}_k^n\,(1 + n\,\epsilon_k/\bar{y}_k) + B + 0(\epsilon_k/\bar{y}_k)^2]. \tag{A5}$$

If we neglect higher order terms in $\epsilon_k/\bar{y}_k$ and take $\bar{y}$ to satisfy eqn (A3) then the propagation of error is given by

$$\epsilon_{k+1} = \epsilon_k\,(1 - nA\,\bar{y}_k^{n-1}\,\Delta t). \tag{A6}$$

Now if we assume that the finite-difference marching scheme is stable if errors do not grow, that is if $|\epsilon_{k+1}| \leq |\epsilon_k|$, then from eqn (A6)

$$\Delta t_s \leq \frac{2}{nA\,\bar{y}_k^{n-1}} \simeq \frac{2}{nA\,y_k^{n-1}} \tag{A7}$$

With the interpretation suggested above for y and A the result in eqn (A7) is essentially the one in eqn (3.2). Stability limits for explicit calculations based on other flow rules can easily be derived in the method outlined above.